Micro Air Vehicle's drag reduction by biplane

Chinnapat THIPYOPAS[1] and Jean-Marc MOSCHETTA[2]
Ecole Nationale Supérieure de l'Aéronautique et de l'Espace (SUPAERO)
10 Av. Ed. Belin, 31055 Toulouse, France

Abstract

As an induced drag is very high for low aspect ratio wing Micro Air Vehicles, the present paper addresses the problem of MAV's drag reduction by using biplane configuration. The single-wing concept and the biplane concept are compared in terms of wind-tunnel measurements and numerical calculations. Then, stagger and gap effects are experimentally investigated including the influence of decalage angle between two wings. Finally, the influent of motor-propeller is presented.

First, low-speed wind tunnel measurements have been carried out in order to compare 16 flat-plate wing models of varying aspect ratios, taper ratios and sweep angles. All models were designed so as to fit into a 20 cm-wide sphere. Lift, drag and pitching moments were measured by a three-component calibrated balance. Wind-tunnel measurements have been compared with simple calculation based on a *Matlab* vortex-lattice code, TORNADO [1]. To account for viscous effects, the skin-friction drag was estimated by a flat plate laminar boundary layer theory based on Blasius formula. The results show a good agreement between numerical calculations and wind-tunnel measurements. The biplane configuration turns out to produce smaller induced drag for a given lift force and also has better lift-to-drag ratio than the monoplane with smaller aspect ratio. A good compromise between cruise performance and manoeuvrability leads to aspect ratios between 2 and 3 for biplane wings. The wind tunnel test was also done with Zimmerman and Plaster planform. Biplane wing has better aerodynamics performance than low aspect ratio monoplane wing.

The effects of gap, stagger and relative angles of attack were studied in a wind tunnel. Longitudinal aerodynamics coefficients have been measured to assess the benefit of positive staggering, evaluate the best gap ratio between both wings and investigate the sensitivity of relative angles of attack onto cruise performances. Results show that gap has very weak influence on the cruise lift-to-drag ratio. Parasite drag can be reduced by a positive relative angle of attack (the upper wing has a greater angle of attack than the lower wing) but then it stalls first. Finally with same dimension, a positive stagger and little negative decalage angle improve the biplane aerodynamics performance. The last section, an influence of a propeller was investigated in a wind tunnel test. As the size propeller is large comparing with MAV, a propeller has high influent to aerodynamics characteristics.

Keywords
Micro Air Vehicles, Biplane Aerodynamics, Gap effect, Stagger effect, Propeller's Influent

1 Introduction

When designing a single-fixed wing Micro Air Vehicle under stringent maximum dimension constraints, one usually ends up with overall aspect ratios of the order of 1-2. This is due to the fact that low-aspect ratios would lead to higher wing area in order to produce a lift force enough for cruise regime. While the induced drag for a well-designed classical airplane at cruise conditions typically represents about 50% of the total drag, the situation is quite different for low-aspect ratio wings of MAVs for which the induced drag can represent as much as 85% of the total drag. Yet, low aspect-ratio wings yield higher maximum lift coefficients [2], resulting in better manoeuvrability. The idea of the present study is to investigate the concept of a biplane which had been study since the early state of flight [3]. Under the same maximum dimension restriction, a second wing obviously increases the friction drag and a parasite drag associated with the additional structural frame. However, it might decrease the induced drag by a factor of 2.

Preliminary calculations based on approximate methods show the benefit of a biplane wing over very low aspect ratio monoplane wing in the following table.

Table 1.1: Skin friction and induced drag by simple approximate methods

case	a.) AR1	b.) AR2	c.) 2 x AR2	
				total
Surface	S	S/2	S/2	
Lift for each wing	W	W	W/2	
Max. Lift	L	L/2	L/2	L
Lift coef.	C_L	$2C_L$	C_L	
Skin friction drag	D_f	$D_f/\sqrt{2}$	$D_f/\sqrt{2}$	$D_f \times \sqrt{2}$
Induced drag coef.	C_{Di}	$2C_{Di}$	$C_{Di}/2$	
Induced drag	D_i	D_i	$D_i/4$	$D_i/2$
Total drag	$1.5D_f + D_i$	$1.5D_f/\sqrt{2} + D_i$		$1.5D_f \times \sqrt{2} + D_i/2$

In table 1.1, three cases of MAV are compared at the same cruising conditions (total weight of 80 grams at 10 m/s): (a) monoplane wing of aspect ratio 1, (b) monoplane wing of aspect ratio 2, and (c) biplane wing of aspect ratio 2. The weight of 80 grams resulted from previous MAV studies carried out at SUPAERO, including all components such as : battery, motor, servos and camera [4].

For a given span, a higher aspect ratio wing yields a smaller total drag due to a smaller wetted area. Yet, for a fixed weight, the induced drag is not changed when the chord is reduced ! This is due to the fact that the angle of attack has to increase to compensate the wing area reduction. However, when reducing the wing area, the lift at cruise conditions becomes too close to the maximum lift, which results in poor manoeuvrability. The advantage of case (c) is that its induced drag is about half the induced drag for a monoplane wing for a given lift. Each wing operates at a lower aerodynamic load and cruise conditions are

[1] Graduate student, Department of Aerodynamics, SUPAERO; chinnapat@hotmail.com
[2] Associate Professor of Aerodynamics, Department of Aerodynamics, SUPAERO; moscheta@supaero.fr.

now relatively far from the stall condition. Naturally, a biplane configuration produces a parasite drag which is about 1.4 times the skin friction drag of the monoplane wing (a). Furthermore, the biplane configuration (c) gives a lower total drag whenever the induced drag of low aspect ratio monoplane (a) represents more than about 45% of the total drag, which is found to be the case for most MAVs (typically around 75% for aspect ratio 1).

From above idea, a biplane configuration might be interested for our MAVs design (which is under stringent maximum 20 cm. and total weight 80 grams). This paper has both experimental approach and numerical approach for verify our expected. MAV's total drag should be reduced by using biplane concept. The first part is an experimental approach, scale-one wing models were tested in a low speed wind tunnel. Three longitudinal aerodynamics characteristics were measured. Second part was done with a numerical approach. Wing planform optimizations are also investigated in these first two parts. And the last section is studying of biplane combination effect by experimental.

2 Wing planform optimization

The goal of section 2 and 3 is to study the effect of the wing planform in view of optimizing a biplane MAV configuration. Following Taguchi's method, a number of geometrical effects have been considered to determine the wing planform which would produce the lowest amount of total drag for a given lift at fixed cruise speed and overall dimension. Wing shape parameters include: aspect ratio, taper ratio, and sweep angle at quarter chord. A total of 16 models were realized so that the each wing fits into a 20 cm diameter disc. Therefore, increasing the aspect ratio implies a dramatic decrease of chord and area. Also, increasing the sweep angle might slightly decrease the wing span and the area for a fixed chord. Aspect ratio ranges from 1 to 4, taper ratio from 0.2 to 1 and sweep angle from 0 to 50 degrees. Wind tunnel measurements as well as approximate numerical methods were used to assess the different models in terms of longitudinal aerodynamic performance. The cruise conditions are defined as a cruise speed of 10 m/s and a weight of 80 grams. For manoeuvrability and safety, the maximum lift (stall condition) should not be less than 2 times the lift at cruise conditions.

3 Wind Tunnel Measurements

3.1 Experimental Methodology

Wind tunnel:

An experimental for this phase was done in a close loop low speed wind tunnel at the Aerodynamics Laboratory of SUPAERO which illustrated on figure 3.1.

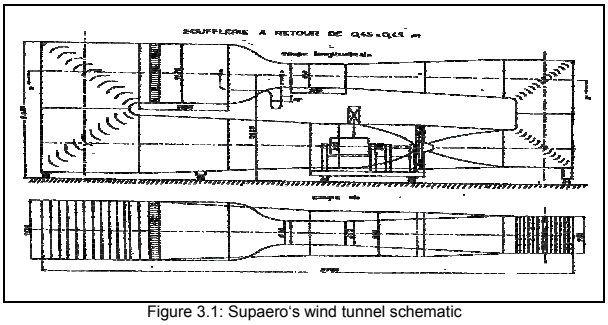

Figure 3.1: Supaero's wind tunnel schematic

The test section is 45 cm x 45 cm.^{2} with a length of 70 cm. The contraction ratio is 6.2. The flow in wind tunnel is conducted by an electric motor. Flow speed can be adjusted by control the motor speed. The maximum speed is 45 m/s. Speed measurement is performed through a Pitot pressure tube located at the beginning of the wind tunnel test section. Both total and static pressure tubes are connected with a pressure transducer to measure the actual dynamic pressure. A series of grids at the beginning of the contraction part gradually splits and damps vortical structures so that the turbulence intensity of the incoming flow is fairly low (~ 1%).

Measurement:

The balance that used in this project is a three-component balance : lift, drag and pitching moment can be simultaneously measured. The balance is also equipped with a motor which is used for changing the model angle of attack. Models are mounted on struts whose drag has been carefully measured as a function of the angle of attack. The lift, drag and moment axes are totally independent.

Figure 3.2: Wind tunnel and data acquisition unit

The angle of attack is controlled manually with the incidence controller. The angle can be adjusted from –30 to +45 degrees but it was used in the range of –10 to stall angle in the present study.

Data acquisition:

The signals from the strain gauges were measured with very sensitive instrumentation using a full Wheatstone bridge configuration. The output signals were read with an instrumentation amplifier circuit, with available gains from 1 to 1000. The amplified analog signals were sent to the computer where they were then converted using a five-channel converter. Five data channels (dynamic pressure, drag, lift, pitching moment and angle of attack) could be measured. All the data was acquired using a PC-base data acquisition system running the code that link with MS-Excel. Before measuring any aerodynamic force and moment with the balance, the amplifier gains were adjusted to minimize the error. The balance was then calibrated using known masses.

Models (Flat plate):

The wing model which dimension is limited at 20 cm. maximum is made of a composite fiber-glass resin. To avoid the influence of wing flexibility, three layers of fine fiber-glass type and two layers of thick fiber-glass have been applied. The resulting wing models are semi-rigid so that no deformation could be observed for an aerodynamic load associated to a speed of 10 m/s. In order to simplify the wing planform selection, a flat-plate airfoil is used for all 16 models. The airfoil is 1 mm thick with a leading edge radius of about 0.5 mm. The trailing edged is linearly tapered over a length of 1 mm.

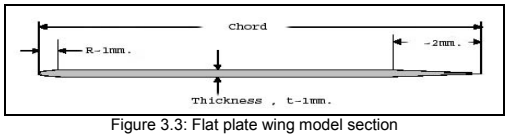

Figure 3.3: Flat plate wing model section

16 models of various trapezoidal planforms were tested. Their parameters are shown in table 3.1.

Table 3.1: List of flatplate wing models

No.	Model Name	Span (cm.)	MAC (cm.)	Area (cm^2.)
0	Disc	20.0		314.2
1	A1S0T0.2T0	12.0	12.0	144.0
2	A1S0T1 T0	14.1	14.1	200.0
3	**A1S25T0.6 T0**	**14.9**	**14.9**	**224.8**
4	A1S50T0.2 T0	12.0	12.0	144.0
5	A1S50T1 T0	11.4	11.4	130.2
6	**A2.5S0T0.6 T0**	**19.1**	**7.6**	**146.7**
7	A2.5S0T1 T0	18.5	7.4	137.9
8	**A2.5S25T0.6 T0**	**19.1**	**7.6**	**146.7**
9	A2.5S25T1 T0	18.5	7.4	137.9
10	A2.5S50T1 T0	16.0	7.1	102.9
11	A4S0T0.2 T0	19.9	5.0	99.3
12	A4S0T1 T0	19.4	4.8	94.1
13	A4S25T0.6 T0	19.6	4.9	96.6
14	A4S50T0.2 T0	18.3	4.9	84.1
15	A4S50T0.6 T0	17.8	4.9	79.5
16	A4S50T1 T0	17.5	4.3	76.7

Note: Model name is coded by wing planform characteristics;
A = Aspect ratio, S = Sweep angle
1st T = Taper ratio, 2nd T = Twist angle
For example : A2.5S25T0.6 is a wing with aspect ratio 2.5, swept 25 degrees at ¼ chord, and taper ratio 0.6

Examples of flat plate wing models are shown on Fig. 3.4.

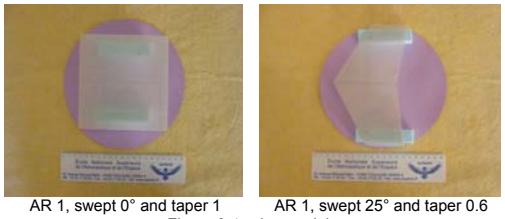

AR 1, swept 0° and taper 1 AR 1, swept 25° and taper 0.6

Figure 3.4: wing models

A recent study of Mueller showed that a curve plate airfoil has greater aerodynamics performance than a flat plate airfoil [5, 6]. The two best wings were also realized using a camber airfoil. The mean camber line follows the Göttingen 417A profile whose coordinates are given in table 3.2. Also, to determine the effect of winglets, the aerodynamics characteristics of 6 curve plate wings with / without winglets were measured.

Table 3.2: Show the wing section and coordinates of the curve plate airfoil

Wing section coordinates

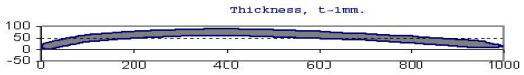

X	Y	X	Y	X	Y
0	0	200	48.35	800	28.00
25	9.25	300	57.00	900	13.25
50	18.00	400	59.00	950	6.25
75	26.25	500	55.50	1000	0
100	33.50	600	49.50		
150	42.25	700	40.00		

Figure 3.5: Curve plate wing model (A2.5S25.T0.6T0)
Left: No winglet, Middle: Upper winglet, Right: Lower winglet

Three struts are inserted through the test section wall to support the model. The measured forces and moment include the struts and their interaction. In order to measure the net force, some correction is necessary. For instance, the drag force from the three struts without the presence of the wing model was measured before each model test. Then, the drag of model has been corrected by

$$Drag_{model} = Drag_{total} - Drag_{strut}$$

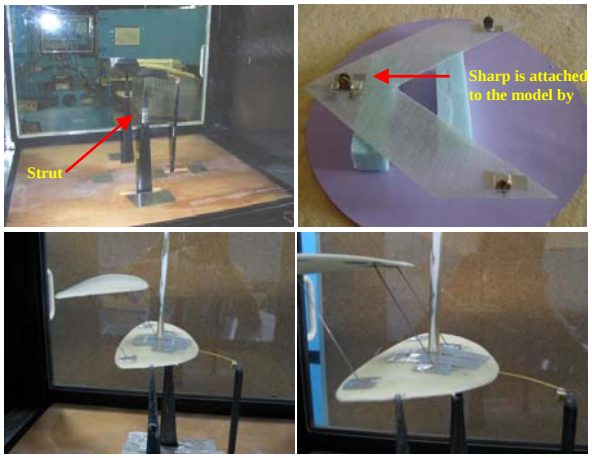

Figure 3.6: Above-Left: Three struts that insert into test section,
Above-Right: Sharp that attaches to model
Below: Measurement of influent of model to drag of strut

In order to verify this equation again, the strut's drag by present of wing model was measured and compared with the strut's drag without present of wing model. Wing model is supported by another strut from ceiling of test section. The apparatus's set up are shown in figure 3.6c and 3.6d. Several incidences were compared and it is found that the strut's drag of both cases is very close. The different is less than 1% of strut's drag.

To compare more easily the different wings, the same reference length and reference area were used to calculate the aerodynamic coefficients (lift, drag and pitching moment coefficients). The reference area is that of a squared wing (aspect ratio 1) which fits into a 20 cm-diameter disc. Its area is 200 cm^2. A reference length of 20 cm is used to calculate the moment coefficients. The pitching moment is measured with respect to the wing leading edge in the symmetry plane.

3.2 Results and Discussions

All results are detailed in table A1 in appendix.

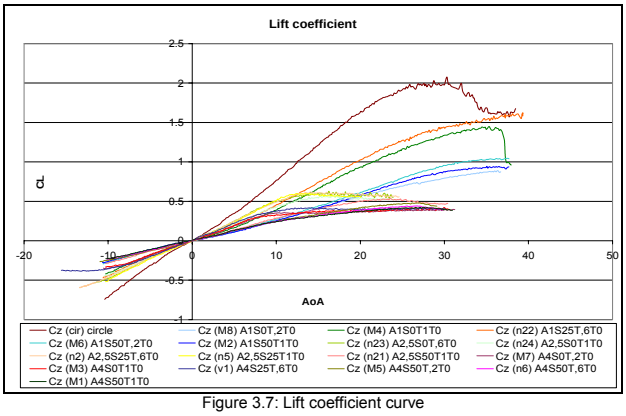

Figure 3.7: Lift coefficient curve

As expected, the wing lift curve slope (Fig. 3.7) is mainly a function of the aspect ratio [7]. This is due to the high influence of the wing tip vortex. Low aspect ratio wings stall at very high angle

of attack. The wing tip vortex which covers all area of a very low aspect ratio wing (AR 1) creates a large downwash velocity. This typically delays the stall angle to about 35–40 degrees. Comparing with the same reference area (200 cm^2), wings of aspect ratio 1 produce the highest lift coefficients. They can produce a lift up to about 160 grams while other wings (AR 2.5 and 4) barely reach half that value. The sweep angle has very low influence on the maximum lift coefficient.

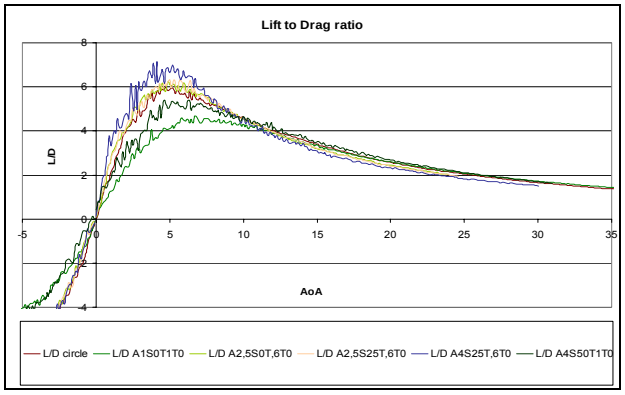

Figure 3.8: Lift to drag ratio curve

Fig. 3.8 illustrates that although low aspect ratio wings provide higher maximum lift coefficients, they usually produce lower maximum lift-to-drag ratios. While L/D ranges about 4-5 for aspect ratio 1, one can reach L/D up to 7 for aspect ratio 4. A wing with aspect ratio 1 having a larger wetted area also yields a greater drag force.

The induced drag factor K is decreased when the wing aspect ratio increases. Low aspect ratio wings (such as AR1) have very high induced drag factor. Increasing the aspect ratio can significantly reduce this factor as illustrated on table 3.3.

Table 3.3: Induced factor for different aspect ratios

AR	1	2.5	4
Factor K	0.4157	0.2937	0.2668

Because of dimension constrain, a good wing planform design is very important. Fig. 3.9a and 3.9b show the impact of taper ratio on the wing design. Wing model A1S0T0.6 has the best performance within aspect ratio 1 wings. It also has the largest wing area. Model A1S0T0.2 has too much taper so it has a smaller area. Its area is actually limited by the leading edge and the trailing edge as marked by red circles in Fig. 3.9a. It has poor performance.

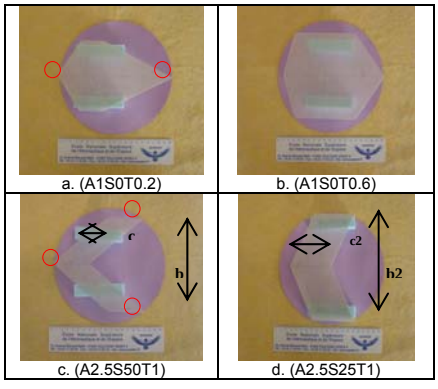

Figure 3.9: MAVs's wing area is limited cause taper and swept angle

Excessive sweep angle tends to decrease the wing area as shown in figure 3.9c. The wing fits in the reference circle by 3 points (both wing tips and the leading edge). Both chord and span are then shorter than the wing shown on fig. 3.8d. which finally results in an increase of the cruise lift coefficient. Consequently, the induced drag is now inversely proportional to the wing area since the induced drag factor K is not much affected (same aspect ratio)

$$C_{Di} = K.C_L^2, \quad C_L = W/(q.S), \quad D_i = q.S.C_{Di}$$

Then $$D_i = K.W^2/(q.S)$$

When using a curve plate airfoil, L/D slightly increases. The maximum lift coefficient increases by a factor of 50% if compared to a flat plate wing. The parasite drag of a curve plate is also higher than of a flat plate one. The main drawback of camber airfoils is that they involve negative pitching moments so that double camber is required to balance the MAV.

3.3 Other wing planform

The previous section interests on simple wing planform shape and it shows the advantage of biplane wing, wing's aerodynamics performance is progressed by increasing aspect ratio and adding another surface. To improve more lift-to-drag ratio, other wing planform which has more efficiency will be discussed in this sub-section. Four wing planforms were observed, Zimmerman, inverse Zimmerman, Plaster and Dynaline. The last two planform are the form of SUPAERO's MAV which have been fly. All planform and their characteristics are shown in the table below.

Planform	Area (m^2)	$CL_{(max)}$	$CD_{(min)}$	$L/D_{(max)}$
Zim1	0.0264	1.251	0.0533	4.03
Zim2	0.0173	0.586	0.0419	5.21
Zim1Inv	0.0264	0.986	0.0538	3.75
Zim2Inv	0.0173	0.605	0.0344	4.96
Plaster1.4	0.0245	0.909	0.0411	4.92
Plaster2	0.0166	0.605	0.0354	5.47
Dynaline1	0.0273	1.260	0.0528	4.46
Dynaline2	0.0173	0.585	0.0375	4.81

* The number located after the name indicates wing aspect ratio

All results demonstrate the benefit of biplane configuration. Induced drag reduces and parasite drag increases but the overall drag decreases. The maximum lift-to-drag ratio rise about 30% for Zimmerman and Inverse-Zimmerman.

4 Numerical Calculations

4.1 Airplane drag

The drag of a classical airplane at subsonic speeds can be traditionally divided into lift-induced drag and minimum drag. Minimum drag is further divided into friction drag, profile drag, and interference drag. The total drag can then be written as :

$$D_{total} = D_{min} + D_{induced} = \{D_{friction} + D_{profile} + D_{interference}\} + D_{induce}$$

For standard airplanes, about two-thirds of subsonic minimum drag may be attributed to skin friction [8, 9]. The remaining drag is due to form drag and interference.

Skin-friction drag:
The simplest method to predict the skin-friction drag coefficient is given by using a theory of flat-plate boundary-layer. The exact solution to the laminar boundary-layer equations for zero pressure gradient solved by Blasius

$$C_f = 1.32824 / \mathrm{Re}^{1/2}$$

Where $\mathrm{Re} = U_\infty l / \upsilon$ and l is the distance from the stagnation point to the transition zone. While in the turbulence regime, the skin-friction coefficient is given by

$$C_f = 0.33333 / \mathrm{Re}^{5/6}$$

Transition takes place when the length Reynolds number nominally exceeds 3.5×10^5 to 10^6 for a flat plate. This critical Reynolds number is often assumed to be about 5×10^5.

Form drag:
It results from flow over curved surfaces, effects of nonzero pressure gradient, and flow separation induced by viscous effects.
The prediction of the form drag, or FF, is obtained by empirical correlations as given by DATCOM, Hoerner, and others. Example for airfoils:

$$FF = 1 + K_1(t/c) + K_2(t/c)^2 + K_3(t/c)^4$$

Where K_1, K_2, K_3 depend on airfoil series. In this case, K_1, term represented the frontal area on which the pressure is acting, is equal to 1.2 and K_3, term represented effect of adverse pressure gradient, is equal to 70 while K_2 is zero [10].

Camber and twist in the wing also increase the form drag accounts, for the fact that all aircraft components are not mounted relative to each other to attain zero lift simultaneously. This increment is related to the drag-due-to-lift methodology.

$$C_{D_{camber}} = \frac{1}{1-e} K (C_L)^2$$

Interference drag:
The mutual interaction of the flow fields developed by the major configuration components is the cause of an interference drag. Interference can be unfavourable with a total drag increase in which the sum of component drags is greater than the total drag of the configuration.
The summation of form drag and interference drag can be approximated by the half of the skin friction drag over the airplane as recommend by [8, 9].

The equivalent skin-friction drag:
The equivalent skin-friction coefficient, C_{fe}, is a convenient method to relate total drag (minimum drag), including form and interference drag, to wetted area.

$$C_{fe} = D / qS_{wet}$$

Lift-induced drag:
Classical aerodynamic theory predicts that the induced drag is given by

$$C_{D_i} = C_L^2 / \pi . e . AR$$

For an elliptic spanwise lift distribution, the wing efficiency factor (e) is equal to one. For a non-elliptically loaded wing, such as tapered and swept wings, this factor is less than 1.

4.2 Calculation Methodology

Vortex lattice methodology is used in this study using the code TORNADO [1] in which viscous effects have been included.

Following the same strategy, a series of swept wings have been analyzed through TORNADO and the computation of parasite drag. Aspect ratio, taper ratio and wing sweep angle were chosen so as to correspond to the experimental models. Additional investigations were performed by considering the following values for aspect ratios : 1, 2, 3 and 4, taper ratios : 0.4, 0.6, 0.8 and 1 , the quarter chord swept angle: 0, 15, 30 and 45 degrees. Finally, a total of 64 wing models which all fit into a 20 cm.-diameter circle were compared in terms of lift to drag ratio.

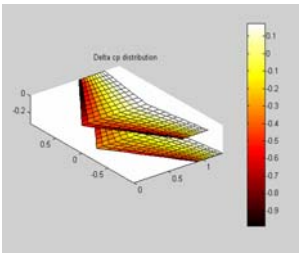

Figure 4.1: Pressure distribution on wing surface by TORNADO code, vortex-lattice computation

4.2 Results and Discussions

The results calculated by the vortex lattice method including the flat plate skin friction drag, are shown on fig. 4.2. For wings of aspect ratio 1, only the L/D ratios for a monoplane configuration are plotted. For other aspect ratios, e.g. 2 to 4, the results are plotted in both monoplane and biplane configurations. The lower L/D values correspond to monoplane configurations while the higher values (red symbols) correspond to biplane configurations. Biplane configurations have the same overall dimension as the monoplane configuration. It appears that higher aspect ratio monoplane wings have better aerodynamics performance at cruise condition (fixed lift force of 80 grams). Lift to drag ratio 5 can be obtained by wings of aspect ratio 1; L/D can reach 7 for wings of aspect ratio 2 and L/D still increases to around 8.5 for wings of aspect ratio 4.

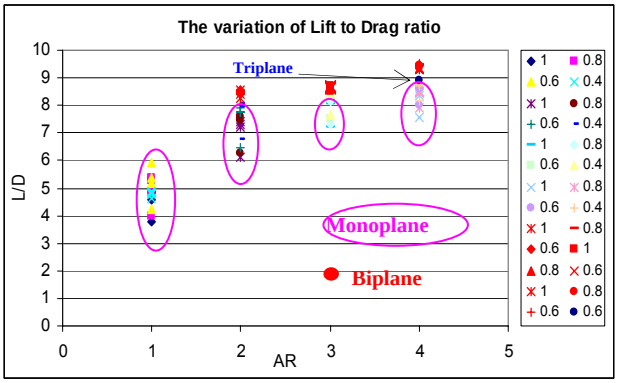

Figure 4.2 (Right): L/D, the red points illustrate the biplane wing L/D

The minimum drag, which almost comes from the skin friction drag or two-third of minimum drag, of low aspect ratio wing is little bit larger than one of high aspect ratio wing. Although the minimum drag coefficient of short chord or high aspect ratio wing is bigger than that of wide chord or low aspect ratio wing, the large wing area of low aspect ratio is more important. The result is it is better in the drag force.

As expected, increasing the aspect ratio can dramatically improve the wing efficiency factor 'K' which can be reduced by a factor of 2 to 4 when the aspect ratio increases from 2 to 4. However, the resulting induced drag force does not perform as good as the wing efficiency factor since the wing area is smaller. Therefore, high aspect ratio MAVs need higher intrinsic lift coefficients and, consequently, produce higher intrinsic induced drag coefficients. In terms of forces, it is still beneficial to reduce the chord length provided that a sufficient manoeuvrability margin is maintained.

For a given aspect ratio, the biplane configuration only slightly improves the lift-to-drag ratio. This is due to the fact that the wetted area is now doubled and the minimum drag for a high aspect ratio biplane is greater than the one associated with a monoplane of aspect ratio 1. Furthermore, the lift does not double by adding one wing because of unfavorable interaction between

wings. Because of a higher performance in induced drag, the biplane configuration is still better than the monoplane wing with identical aspect ratio and that the monoplane with aspect ratio 1. A triplane configuration of aspect ratio 4 was calculated and plotted on Fig. 4.2 (dark-blue point). Its lift to drag ratio is smaller than of biplane configuration because of excessive parasite drag.

As a conclusion to the numerical study:

1. Wings of aspect ratio 1 can fly at the prescribed cruise conditions with sufficient margin between cruise conditions and stall.
2. Monoplane wings of aspect ratio 4 wing cannot meet the cruise conditions since the wing stalls before producing 80 grams of lift force.
3. Using aspect ratio 2 to 3 in monoplane concept, a 80 grams MAV can fly, but it flies fairly close to the stall angle, especially for aspect ratio 3. Aspect ratios for a practical monoplane MAV should not exceed 1.8-2.
4. The triplane configuration with aspect ratio 4 is acceptable for flight but its lift to drag ratio is not better than in the case of a biplane at lower aspect ratio.
5. The interesting region for a biplane MAV is found for wing aspect ratios ranging from 2 to 3. Although the margin of maximum angle of attack and angle at cruising is still less than 2, it is not far from it. With a good selection of wing relative position, stagger and decalage, adding appropriate winglets and taking into account the propeller effect, biplane wings can be considered as promising candidates for practical MAV applications.

Table 4.1 compares three configurations of equal maximum dimension: (a) a monoplane wing of aspect ratio 1, (b) a monoplane wing of aspect ratio 2, (c) a biplane wing of aspect ratio 2. Stall lift values were obtained from wind tunnel measurements while cruise values were computed through the vortex-lattice method corrected with viscous effects.

Table 4.1: Lift and Drag force at cruising condition

AR	Config-uration	Stall	Cruise (10 m/s and weight 80 g)					
		L(max) [g.]	L [g.]	D [g.]	Do [g.]	Di [g.]	L/D	Di/D
1	Monoplane	148.5	80.0	13.5	1.90	11.6	5.93	85.9
2	Monoplane	95.98	80.0	10.1	1.72	8.42	7.89	83.1
2	Biplane	158.3	80.0	8.7	3.44	5.32	9.13	60.8

Based on table 4.1, conclusions can be summarized as follows:

- For a given maximum overall size and a fixed lift force at cruise conditions, a biplane concept provides lower drag (35% reduction) by reducing the induced drag by a factor of 2 and increasing the parasite drag by 80%.
- Stall lift force does not significantly benefit from the biplane concept with only a slight increase of 6% in maximum lift.
- Cruise lift-to-drag ratio can be increase by 53% when using a biplane wing.

5 Biplane Effect

5.1 Experimental Methodology (scale 3)

This section presents the effects of biplane wings combination in terms of gap, stagger and decalage angles. Two identical wings based on the best monoplane wing have been used. The study was done at S4, an Eiffel wind tunnel type of ENSICA, Toulouse. S4 is an elliptic open test section size 2m x 3m which has speed range from 10 to 40 m/s. The flow is generated by three motor-turbines, 90 kW of power. The test can be both force measurement and visualization. S4 is constructed by wood and fiber-glass contraction ratio 5. The turbulence intensity in test section is order of 0.5% at 20 m/s.

A generic biplane model at scale 3 was fabricated in polystyrene covered with fiber-resin. Each wing is of aspect ratio 3, sweep angle 30 degrees and taper ratio 0.8. A self-stable double camber airfoil was used. The wings have span 575 mm. with can fit into a 60 cm. disc.

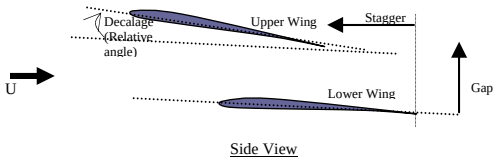

Figure 5.3: Biplane geometrical parameters

To ensure that the biplane model does not vibrate during the test, the upper and lower wings were connected by using two aluminium end-plates at both tip wings and one aluminium ingot size 10 mm x 3 mm at leading part of model. Several end-plates with varying dimensions and shapes were fabricated to suit the different gaps and stagger ratios. Both gap and stagger are referenced by the mean aerodynamic chord (MAC) of the wing which is 192 mm. The stagger ratios are -15%, 0%, +15% and +30% of MAC. Three gap ratios : 0.75, 1.00 and 1.25 were examined. Finally, relative angle settings, or decalage angles were analyzed using -6°, 0° and +6°.

A total of 15 biplane combinations were investigated. The detail of biplane wing model and its combination are shown in the figure 5.3 and table 5.1.

Table 5.1: List of model configurations

No.	Model Name	Gap ratio (G)	Stagger ratio (S)	Decalage angle (i)
1	Monoplane	No winglet		
2	Monoplane	With winglet		
3	G0.75Sn15i0	75%	-15%	0°
4	G0.75S0i0	75%	0%	0°
5	G0.75S15i0	75%	15%	0°
6	G0.75S30i0	75%	30%	0°
7	G1.25Sn15i0	125%	-15%	0°
8	G1.25S0i0	125%	0%	0°
9	G1.25S15i0	125%	15%	0°
10	G1.25S30i0	125%	30%	0°
11	G1S0i0	100%	0%	0°
12	G1S0in6	100%	0%	-6°
13	G1S0i6	100%	0%	6°
14	G1S15i0	100%	15%	0°
15	G1S30i0	100%	30%	0°
16	G1S30in6	100%	30%	-6°
17	G1S30i6	100%	30%	6°

Figure 5.4 shows the model with the support in S4 wind tunnel.

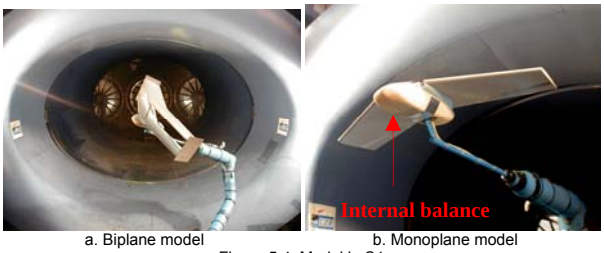

a. Biplane model b. Monoplane model

Figure 5.4: Model in S4

In this study, aerodynamic forces were measured by a 6-component internal force balance. The results are directly corrected and plotted in a computer in the control room. The effect of Reynolds number was studied on the monoplane wing through the use of different freestream velocities : 5, 10, and 15 m/s.

Visualizations were carried out for a single configuration using smoke generation and tuft method. The vortex behind the model was observed by shooting a laser sheet into the flow including smoke. For a tuft method, white strings were attached to wing surface. With the fluorescent light, the stall phenomenon can be observed easily by the video camera located in the wind tunnel section.

5.2 Results and Discussions

Monoplane model:

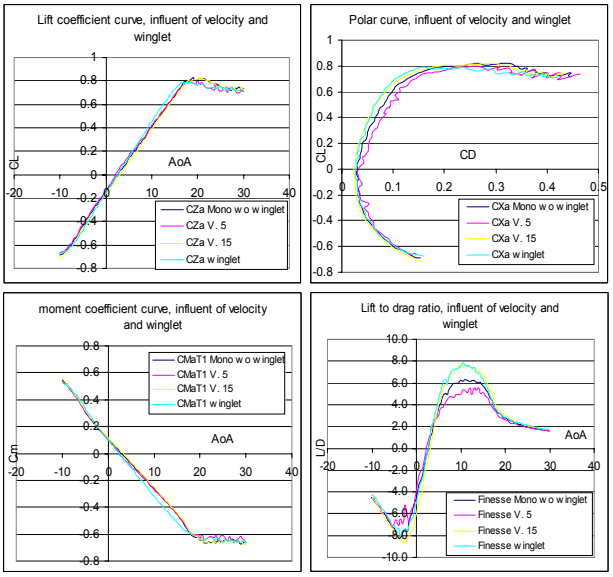

Figure 5.6: An effect of Reynolds number and winglet on monoplane

First, the influence of the Reynolds number has been investigated by using different wind speeds. Fig. 5.6a indicates that the lift curve slope does not change, only stall phenomena at low Reynolds number (velocity 5 m/s) occur a little earlier (1 degree) than at other speeds. At 10 m/s, the wing stalls at 19 degree of incidence. The zero-lift drag increases as the Reynolds number is reduced. The lift to drag ratio curve on fig. 5.6d clearly illustrates the reduction of wing performance with the Reynolds number. The winglet added to the wing is small compared with wing surface so that the parasite drag does not change much. If the overall dimension is fixed, the total drag can benefit from the addition of winglets since the winglet model (green line) produces a higher lift-to-drag ratio if compared with a wing without winglets (blue line).

Influence of Gap:

Maximum lift coefficient now reaches 1.5. Higher gap ratio reduces the interaction between both wings. The lift curve slope and the maximum lift also increase. After stall, lift is decreased for a monoplane wing while for biplane, the lift still increases after the stall of the upper wing at 18 degrees. While the parasite drag increases for the biplane wings (due to the increase of wetted area and end-plates), the induced drag factor is lowered. The gap does not affect the lift-to-drag ratio. The maximum lift-to-drag is order of 6 which is same as found in monoplane. It is different from the one calculated by the vortex lattice method plus skin-friction correction in the previous section. This may come from the skin-friction drag of the endplates and the drag of ingot. One test was done at zero angle of attack to observe the drag of this ingot connector, 10% reduction of parasite drag is found. By subtracting this drag, the maximum lift-to-drag ratio will multiply by 11%.

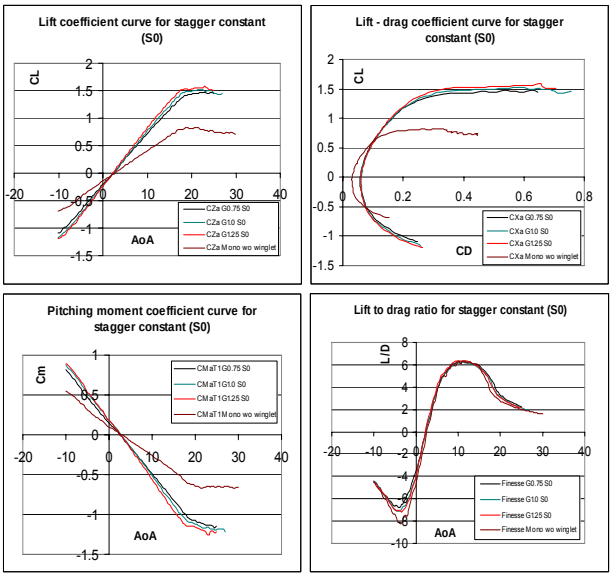

Figure 5.7: An influence of gap between two wings

Influence of Stagger:

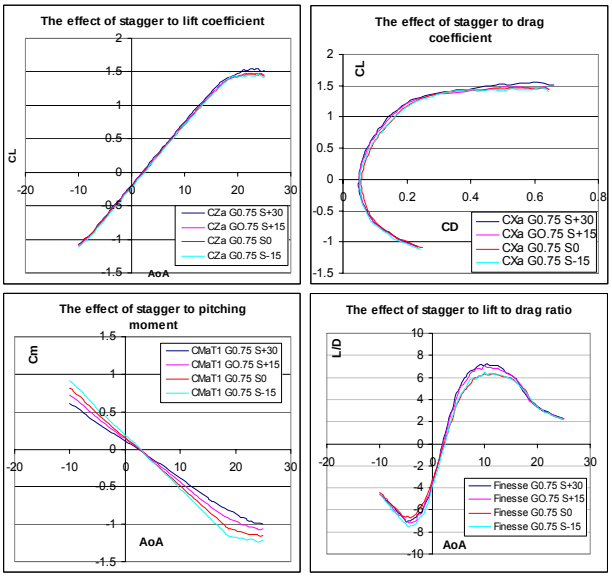

Figure 5.8: Stagger effect over the aerodynamic characteristics of biplane

Figure 5.8 shows the effect of stagger in biplane configuration. The stagger has no significant effect on the lift curve slope (Fig. 5.8a). The maximum lift for a stagger of +30%MAC (blue line) is slightly improved. The zero-lift angle of attack shifts with the stagger. The local angle of attack of the upper wing is artificially increased by the presence of the lower wing [11]. Therefore, the upper wing has more efficiency than lower one [12]. Its zero-lift angle of attack decreases with moving upper wing forward. Besides, a negative stagger combination results in higher zero-lift incidence. Stagger reduces the parasite drag. This affects the lift-to-drag ratio of biplane wings: L/D increases from 6.3 to 7 by a positive 30%MAC stagger. This trend

is consistent with [13]. The stagger has more influence to aerodynamics performance than the gap between two wings. The moment shown in figure 5.8c is the pitching moment at leading edge of lower wing. It was found that the moment at aerodynamics center point of biplane, moment at zero lift angle, does not change.

Influence of Decalage:

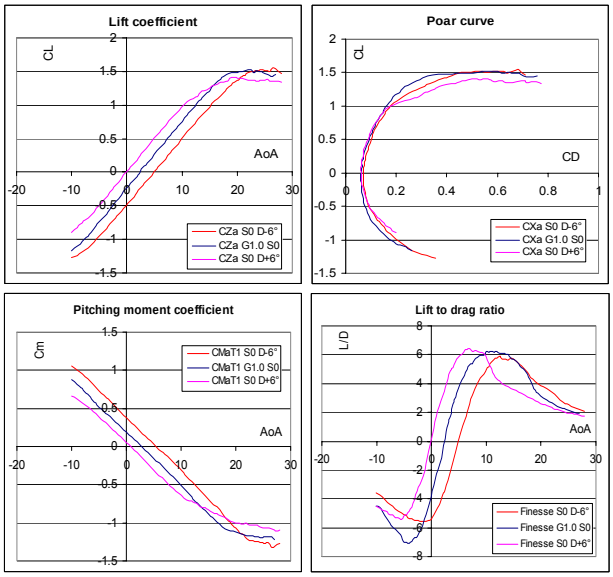

Figure 5.9: Effect of decalage angle (Configuration gap 1, stagger 0)

Three angle of wing decalage were investigated : -6°, 0° and +6°. The zero-lift angle is moved as an effect of the overall camber line. With a decalage of 6 degrees, the lift curve is parallel to the other curves for low angles of attack (until 12 degrees). The first change in lift slope corresponds to an actual angle 18 degrees of the upper wing (12 degrees of model plus 6 degrees of setting angle) where the upper wing stalls. A second stall occurs at 20 degrees where the lower wing stalls. The trends of lift curve of 0° and -6° degrees decalage do not differ significantly. Maximum lift-to-drag ratios of all three combinations are very close. The maximum lift coefficient might increase by using a negative decalage if both wings stall at the same time. This would improve the natural stability of the biplane but would imply a sudden stall phenomenon.

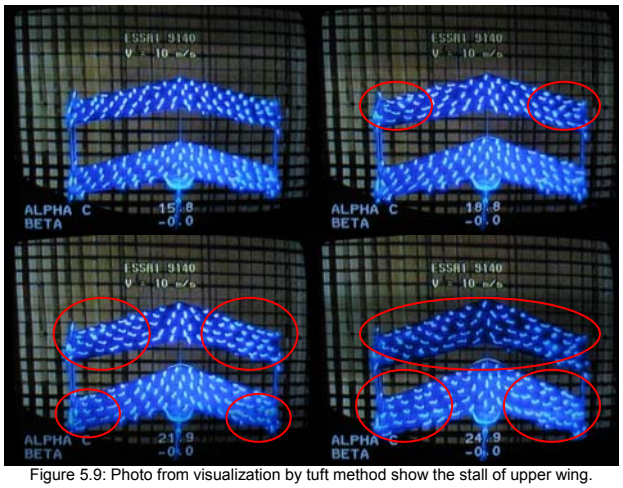

Figure 5.9: Photo from visualization by tuft method show the stall of upper wing.

Boundary layer separation on the wings has been observed by the tuft method. The upper wing in positive stagger configuration stalls before the lower one since the circulation of the lower wing creates an upwash velocity component on the upper. Furthermore, the lower wing is affected by the upper wing in the opposite direction [11, 12]. That is why the upper wing stalls before the lower wing. It can also explain the decrease of maximum lift in positive decalage angle as shown in fig. 5.9a.

Endplates:

Figure 5.11 shows the photo of endplates connector and bar/winglet connector.

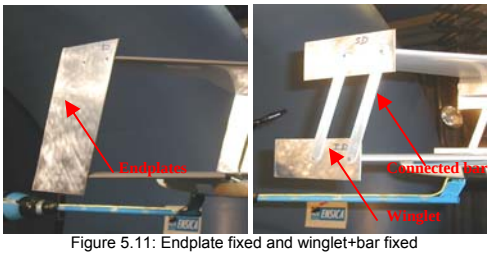

Figure 5.11: Endplate fixed and winglet+bar fixed

The influence of end-plates and winglet was tested with the configuration G1S30i0 as shown in figure 5.10. It is found that, for longitudinal characteristics, winglets and end-plates have the same efficiency. With a smaller wetted area the parasite drag of a biplane-winglet configuration was expected to be less that the parasite drag of endplates. In practice, the parasite drag does not differ because of the drag of four bars linking both wings. Also, the presence of end-plates degrades lateral stability.

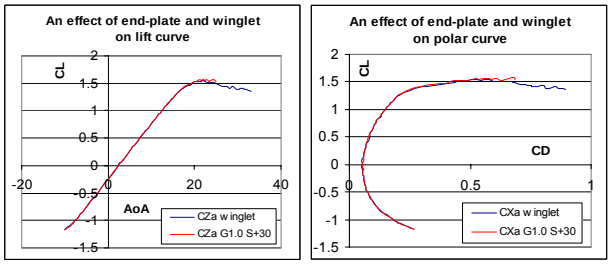

Figure 5.10: Aerodynamics result for endplate and winglet model.

5.3 Swept wing (scale 1)

Biplane effect with a swept wing scale 3 had been discussed in previous section. In this section, biplane configuration is applied to a swept wing scale 1 (maximum dimension 20 cm.). The experimental was set up at Aerodynamics Laboratory, SUPAERO. Both wings are attached by using four cylinder metals diameter 0.8 mm. Gap, stagger and decalage angle are variable.

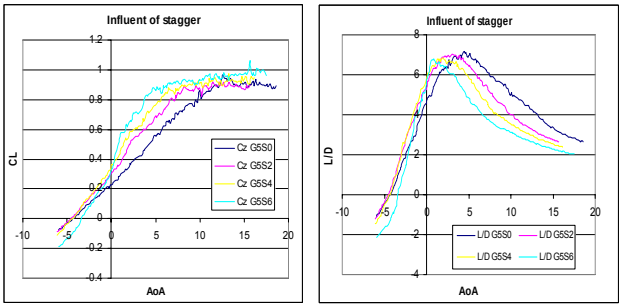

Figure

The influent of gap ratio in model scale 1 is similar as in scale 3. Higher gap give higher lift force but it dose not change wing's maximum lift-to-drag ratio. On the other hand, not as in scale 3 model, lift curve for scale 1 model is changed with a stagger of wing. The effect of stagger between two wings is difference that found in scale 3. The slope increases with stagger positive. And it stalls early than no stagger model. This can be explained that the upper wing stalls at low angle of attack. The local incidence angle of the upper wing is higher than airplane incidence. This is due to the circulation flow from the lower wing. It does not occur in scale-3-model because it has two end-plates or winglet. Biplane stagger positive has a little smaller aerodynamics performance than lower stagger.

Decalage angle has a lot effect to aerodynamics characteristic especially the maximum lift coefficient and lift-to-drag ratio. The influent of relative angle between two wings, decalage angle, is presented in figure. The model is the configuration of stagger +4 cm. The angle of attack shown in the curve is the model angle of attack which bases on the lower wing.

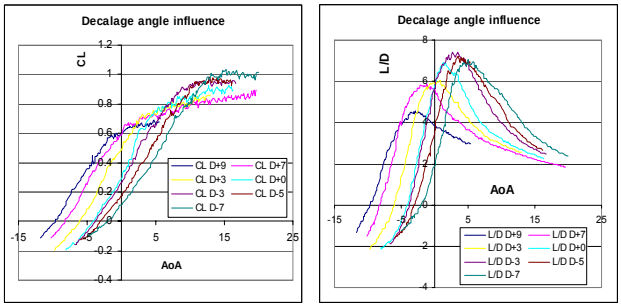

Figure

As known that the upper wing stalls before the other wing, lift curve of configuration positive decalage is beginning to stall very early, for example D+9 stalls at 0°. Model dose not suddenly stall but some lift from lower wing is still developed. Not same as negative decalage (setting angle of upper wing < lower wing), the maximum lift rises to about CL=1, increases 0.1 from no decalage configuration. And the stall angle increase about 7 degrees equal to the decalage angle. The maximum lift-to-drag ratio is also affected by wing decalage angle. The +3° decalage model gives maximum aerodynamics performance.

5.4 Zimmerman and Plastere planform (scale 1)

Zimmerman, Inverse-Zimmerman and Plastere planform which have better aerodynamics performance than a trapezoid shape are analyzed in this section. Four cylinder metals are used for connecting two wings. To ensure the relative angle between two wings, or decalage angle, the vertical length of leading and tailing edge are measured before every experiment. The tandem configuration was also interested by combine Zimmerman and Inverse-Zimmerman.

Gap between two wings affects to aerodynamics characteristics as before. Increasing gap distance reduces the interaction between upper and lower wing. The maximum lift increases with the gap ratio but it has not much effect to lift-to-drag ratio of biplane. The stagger effect is not exactly same as observed in scale 3 at S4. Lift curve of high stagger is not linear as conventional monoplane. The lift curve slope in negative angle of attack regime is smaller than that in the positive regime because high downwash flow from the upper wing affects to lower wing. In another hand, both wings directly pass to the up stream flow field so the positive stagger configuration give higher lift. The maximum lift-to-drag ratio does not much differ for each stagger combination. This phenomenon is not happened on swept biplane wing in section 5.1. Since the wing is swept and two end-plates, downwash flow from upper wing is not affects to lower wing.

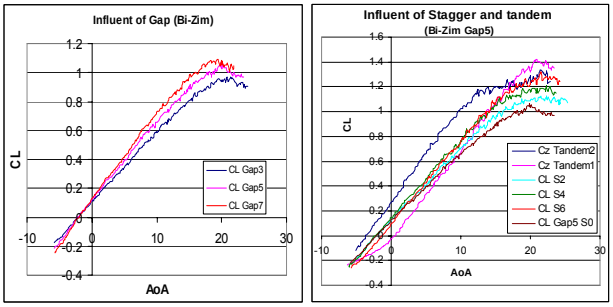

Figure : Lift coefficient curve
Tandem1 is the configuration that fore-wing is above aft-wing.
Tandem2 is one that fore-wing is below aft-wing.

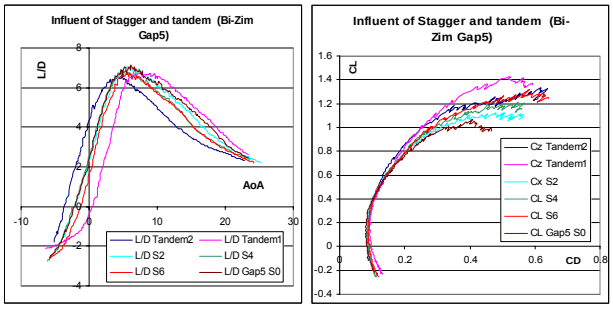

Figure : Lift-to-drag ratio and drag polar (all configuration has gap 5 cm.)

6 Influent of motor-propeller

6.1 Scale 3 model, S4 wind tunnel, ENSICA

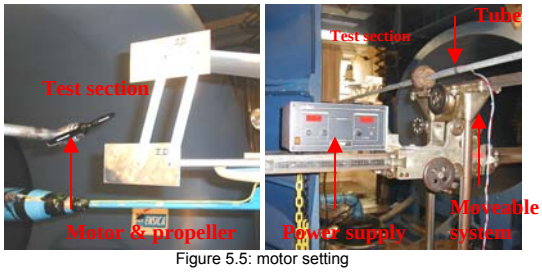

Figure 5.5: motor setting

An electric motor with a propeller has been attached by a tube inserted into the test section so that the motor position is easily adjustable (Fig. 5.5). The influence of the flow induced by the propeller was performed at angles of attack between 10 degrees and the stall angle. Several motor positions in the spanwise direction were studied (Fig. 5.6). The propeller regime was controlled by the power supply amplifier directly connected to the motor. All test were done with the same motor speed at 5.4Volts and 10 Amps.

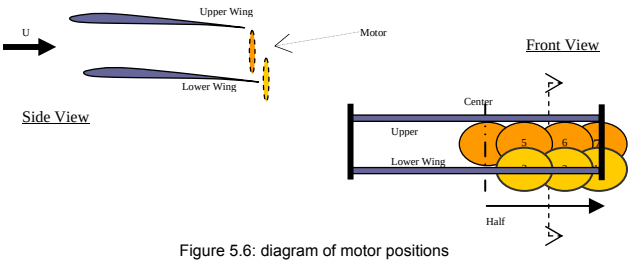

Figure 5.6: diagram of motor positions

Effect of propeller

The effect of motor was investigated on the model G1S30i0 with winglets. Table A2 in appendix gives the results from experimental for the influence of the motor. The values given are expressed as the differences between configurations with and without motor, $(\Delta X = X_{wM} - X_{woM})$. The suction flow created on the wing by the propeller affects the aerodynamics lift force. Static measurements for angles of attack of 14, 18, 22 and 26 degrees were performed using different motor positions. At 14 degrees of incidence, in the pre-stall regime, the presence of a motor near the lower wing (position 2 & 3) does not affect the aerodynamic forces and moment. Motor position 1 at the wing tip increases the lift and reduces drag because the rotating flow induced by the motor counters the wing tip vortex of lower wing. All motor positions above the lower wing (positions 4 to 7) increase the lift coefficient without changing the model drag. The pressure difference between upper and lower surfaces of the lower wing is larger because its upper surface velocity increases while the total pressure remains constant [14].

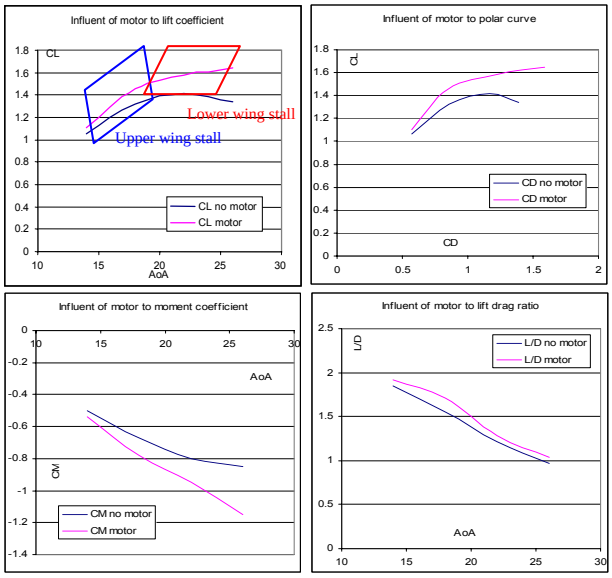

Figure 5.12: The influence of induced flow by motor

In the stall regime, all motor positions increase the lift coefficient of biplane MAVs. For swept wings, separation first occurs in the vicinity of wingtips so wingtip positions are more effective than the center-wing position. Without propeller, the upper wing usually stalls before the lower wing. The effect of the propeller is clearly visible on Fig. 5.12a where an increment of lift appears at angles of attack between 15 and 18 degrees. The drag force is also increased due to induced drag effect but the lift-to-drag ratio is improved (Fig. 5.12d). The pitching moment of the model becomes more negative since the lift increase on the lower wing tends to nose down the model. Finally, motor position 6 which corresponds to a nearly wingtip upper wing position is the best position among the different positions investigated.

6.2 Scale 1 model, at SUPAERO

Inverse-Zimmerman planform was selected to study the influent of flow induced motor-propeller in this step. The experimental in low speed wind tunnel with real scale reduced the correction of Reynolds number effect. The motor Maxon that used for Plaster was used in this experimental because its range is suitable for MAVs. The observation was divided in three parts. First is the flow influence on single wing. Several motor's position are interested. Then the flow induced on biplane was done. In first and second part, motor-propeller is separated from the model, the measurement obtained is the only the wing, thrust from motor is not included. The observation was done by static test for several angles of attack. The last one is the effect of motor-propeller on biplane model.

First, Motor-propeller was designed in different position, traction, and pusher, above wing, in-line wing and below wing. But some position was not measured due to the support of a wing model. An angle of attack measured are at -5°, 5°, 10° and at stall regime; 17°.

Although the results are not very clear, the trend from most result shows that blowing flow, propeller located in front of wing, is better than suction flow. And putting the motor-propeller under wing gives poor advantage.

In second and third observation, the stagger +4 cm. which gives good both in lift-to-drag ratio and maximum lift was used. Gap of biplane 4 cm. was selected to having same as diameter of propeller. Three pusher positions are designed, on the upper wing, on the lower wing and between two wings.

Motor-propeller, then in third part, was fixed to the biplane model on the upper and lower wings. Diameter of propeller 4cm. was performed as in the past measurement. The figure below presents the set up of model in the third part. Motor propeller is attached to the upper wing by using an aluminum scotch tape. Motor was rotating by the current 4.5 Volts, 0.8 Amp.

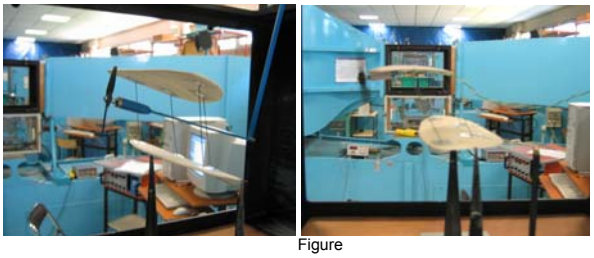

Figure

The results from 2nd and 3rd observe are similar. Only the force in horizontal (drag, thrust) is changed. Aerodynamics characteristics are modified by the flow induced by motor-propeller. But putting motor between two wings gives smallest effect. Lift is increased just a little comparing with the other two positions. While flow induced directly through the upper wing or lower wing has elevate influent on the model especially at stall regime. Lift and drag of both configurations are increased. However their effects do not much differ, except pitching moment. Flow induced on upper wing augments a pitching moment of model since it increases lift and drag on the fore-wing (upper wing), positive pitching.

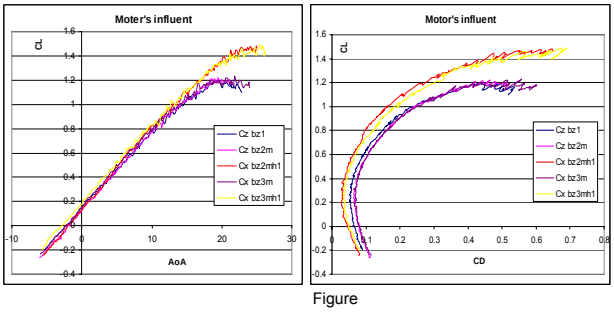

Figure

The results shown in figure is from the third observation, motor is included in the model. The "bz1" is the biplane; "bz2m" remarked the upper wing motor position and "bz3m" is for lower

wing. Red and yellow lines are the 4cm.-diameter propeller at upper and lower wing.

7 Conclusions

Wing planform is very important for MAVs design. The present study showed the benefit of using a multi-plane wing over monoplane wing if the overall dimension is fixed. Because biplane wings can sustain level flight with higher aspect ratio wings, the biplane induced drag force is lower than when using monoplane wing for a given lift force. This conclusion is strongly related to the fact that MAV wings are strictly constrained in overall dimension and weight. Although the parasite drag is significantly increased for a biplane wing, the fact that monoplane MAVs usually operate with low aspect ratio wings makes higher aspect ratio biplane wings more attractive. Both experimental and numerical approaches confirm that a swept-back wing suitable for biplane is a wing with aspect ratio 2.5 to 3, with taper ratio of 0.6 and sweep angle about 30 degrees.

A parameter study, carried out on a scale 3 model, has indicated the general tendencies of the gap effect, the stagger effect and the decalage effect. The advantage of positive stagger has been pointed out. The use of a large gap is not recommended because this means an increase of parasite drag due to larger endplates and a decrease in wingspan if the configuration has to stay within a sphere of constant overall dimension. A negative decalage angle and the presence of a motor significantly the biplane stall. The maximum lift can increase if the stall of upper wing is delayed. For desing purpose, it is still interesting to let the upper wing stall first since it then provides natural longitudinal stability.

Recent wind tunnel and numerical tests have demonstrated that cruise lift-to-drag ratios can be further improved by using optimized monoplane wing planform such as inverse Zimmerman used by Mueller [5] or the Plaster planform devised at SUPAERO by Reyes and co-workers [4] (Fig. 6.1).

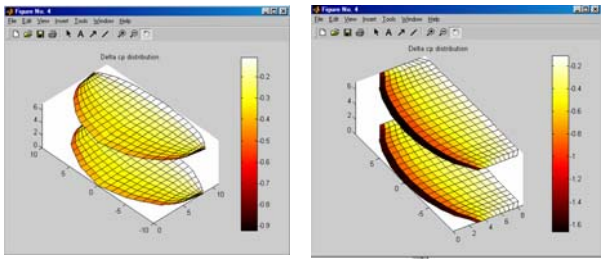

Figure 6.1: Optimized monoplane wing planforms (left: Inverse Zimmerman, right: Plaster)

Numerical computations confirmed by experimental measurements have revealed that lift-to-drag ratios can reach high practical values while maintaining a sufficient margin for manoeuvrability (table 6.1). Three series of wings have been tested : the optimized sweptback wing, the inverse Zimmerman wing and the Plaster wing. For each wing the stagger effect has been analyzed (1 : positive stagger, 2 : no stagger, 3 : negative stagger). The conclusion of these preliminary results is that the Plaster wing (Fig. 6.1, right) yields a stable biplane (positive pitching moment coefficient with respect to the aerodynamic center) with a lift-to-drag ratio of 8.63 and a sufficient margin for manoeuvrability. On-going developments include propeller effect in order to further increase the ratio between stall lift and cruise lift.

Biplane type	L/D cruise	L/D max.	CL_{max}/CL_{cruise}	Cm_0
BSWE1	5.16	5.16	1.71	-0.0371
BSWE2	5.6	5.83	1.64	-0.0260
BSWE3	5.01	5.07	1.54	-0.0042
BPLA1	7.03	7.19	2.04	0.0418
BPLA2	7.89	8.63	2.02	0.0198
BPLA3	6.67	6.76	1.79	-0.0107
BZIM1	6.85	7.07	2.32	0.0603
BZIM2	7.66	7.95	2.06	-0.0347
BZIM3	6.28	6.44	1.87	-0.0165

Table 6.1: Comparison of aerodynamic performance for optimized biplane wings:
BSWE1 : biplane sweptback wing with positive stagger,
BPLA3 : biplane Plaster wing with negative stagger,
BZIM2 : biplane inverse Zimmerman wing without stagger

Acknowledgments

This study could not have been completed without the constant support from the Composite Material Laboratory of SUPAERO where all models were fabricated. The author would like to express their gratitude to Alain Combes, Jérôme Clevers and José Torralba for contributing to the results obtained in section 6 and the S4 wind tunnel staff of ENSICA for their assistance to produce the biplane geometry measurements. Last, all members of the Aerodynamics Laboratory of SUPAERO for their helpful discussions and contributions to the present study.

References

[1] T. Melin, “A Vortex Lattice Matlab Implementation for Linear Aerodynamics Wing Applications”, *Master Thesis*, Department of Aeronautics, KTH, 2000.

[2] G.E. Torres, T. J. Mueller, “Aerodynamics Characteristics of Low Aspect Ratio Wings at Low Reynolds Numbers”, in *Fixed and Flapping Wing Aerodynamics for Micro Air Vehicle Applications*, Ed. T.J. Mueller, Progress in Aeronautics and Astronautics, vol. 195, AIAA Pub., p. 115-141, 2001.

[3] Max M. Munk, “General Biplane Theory: NACA Report No.151”, National Advisory Committee for Aeronautics

[4] Manuel José Reyes Guitiàn, “Development and analysis of a Micro Drone”, *SUPAERO 2001*

[5] Mueller, T.J., “Aerodynamic Measurements at Low Reynolds Numbers for Fixed Wing Micro-Air Vehicles,” *presented at the RTO AVT Course on “Development and Operation of UAVs for Military and Civil Applications,* Rhode-Saint-Genese, Belgium, September 13-17, 1999

[6] Pelletier, A. and Mueller, T.J., “Low Reynolds Number Aerodynamics of Low-Aspect-Ratio, Thin/Flat/Cambered-Plate Wings,” *Journal of Aircraft, Vol. 37, No. 5, pp. 825-832*, September-October 2000

[7] John D. Anderson, “Introduction to Flight, Third Edition”, *McGraw-Hill International Editions,* 1989

[8] John D. Anderson, “Aircraft Performance and Design”, *McGraw-Hill*, 1999

[9] Eugene E. Covert, “*Thrust and Drag: Its Prediction and Verification”*, *Progress in Astronautics and Aeronautics Volume 98*

[10] Hoerner, Sighard F., “Fluid-Dynamic Drag”, *page 6-6*, Hoerner Fluid Dynamics, 1965

[11] V. de Brederode and B. Rocha, “Aerodynamic Interference among Neighbourig Lifting Components”, *published in RTO MP-052*

[12] Richard M. Mock, “The Distribution of Loads Between the Wings of a Biplane having Decalage”, *Technical Notes National Advisory Committee for Aeronautics No. 269*, 1927

[13] F. H. Norton, “The Effect of Staggering a Biplane”, *Technical Notes National Advisory Committee for Aeronautics No. 70*, 1921

[14] Intratep N., “The Investigation of an Inboard-Winglet Application to a Roadable Aircraft”, *Master Thesis,* Virginia Polytechnic Institute and State University, Blacksburg, Virginia, May 2002

Appendix

Table A1: Summary of the measurement result from wind tunnel

No.	Model Name	$C_{L\alpha}$*	$C_{D\min}$	$C_{D\min}$*	$C_{L\max}$	K* (induced drag factor)	AC (cm.)	$C_L = 0.64$			$C_L = 0.32$		
								C_D	L/D	AoA	C_D	L/D	AoA
0	Disc	2.8223	0.0232	0.0147	1.997	0.3578	8.32	0.127	5.052	8.56	0.055	5.871	4.6
1	A1S0T0.2	2.1647	0.0146	0.0202	0.887	0.5127	6.176	0.293	2.209	23	0.085	3.803	12.3
2	A1S0T1	2.5556	0.0219	0.0214	1.449	0.3888	5.336	0.189	3.399	14.6	0.073	4.39	8.56
3	A1S25T0.6	2.4667	0.0112	0.0100	1.621	0.3857	8.926	0.164	3.953	13.5	0.058	5.532	7.56
4	A1S50T0.2	2.4114	0.0163	0.0224	1.046	0.4178	9.967	0.256	2.530	21	0.078	4.128	11.3
5	A1S50T1	2.4902	0.0183	0.0281	0.944	0.3738	7.633	0.252	2.552	21.8	0.081	3.967	12.2
6	A2,5S0T0.6	3.7786	0.0200	0.0273	0.627	0.2814	3.099	-	-	-	0.055	5.899	6.38
7	A2,5S0T1	3.5560	0.0112	0.0162	0.572	0.2966	2.43	-	-	-	0.054	6.036	7.44
8	A2,5S25T0.6	3.6615	0.0172	0.0234	0.619	0.3032	4.904	-	-	-	0.052	**6.288**	6.38
9	A2,5S25T1	4.0961	0.0200	0.0290	0.601	0.2683	4.503	-	-	-	0.061	5.227	6.5
10	A2,5S50T1	3.0513	0.0067	0.0131	0.535	0.3190	5.766	-	-	-	0.071	4.552	11.5
11	A4S0T0.2	4.3273	0.0166	0.0326	0.355	0.2413	2.453	-	-	-	0.060	5.404	8.46
12	A4S0T1	4.5539	0.0167	0.0345	0.381	0.2455	1.497	-	-	-	0.074	4.386	9.83
13	A4S25T0.6	4.9468	0.0133	0.0275	0.418	0.2363	3.261	-	-	-	0.058	5.613	7.6
14	A4S50T0.2	3.3926	0.0124	0.0295	0.481	0.2943	5.221	-	-	-	0.092	3.499	14.3
15	A4S50T0.6	3.4883	0.0095	0.0239	0.442	0.3056	5.95	-	-	-	0.091	3.533	14.9
16	A4S50T1	3.5983	0.0141	0.0368	0.424	0.2781	5.311	-	-	-	0.091	3.508	15.1

Note: * referenced by its area

Table A2: An influence of suction flow by motor

AoA	With Motor									No motor	Motor position 6
	motor ‘s position	1	2	3	4	5	6	7			
14	ΔCL	0.014	0	-0	0.016	0.044	0.042	0.048	CL	1.061	1.103
	ΔCD	-0.01	0.002	-0	0.003	0.02	0	-0	CD	0.574	0.574
	ΔCM	-0.01	0	-0	-0.01	-0.03	-0.04	-0.04	CM	-0.5	-0.54
18	ΔCL	0.052	0.052	0.034	0.027	0.084	0.128	0.092	CL	1.327	1.455
	ΔCD	-0.01	-0.01	-0.02	0.001	-0	-0.002	0.004	CD	0.854	0.852
	ΔCM	-0.04	-0.03	-0.02	-0.02	-0.06	-0.11	-0.08	CM	-0.67	-0.78
22	ΔCL	0.08	0.072	-0.01	-0.015	0.034	0.166	0.146	CL	1.416	1.582
	ΔCD	0.036	0.032	0.03	0.023	0.032	0.064	0.054	CD	1.167	1.231
	ΔCM	-0.08	-0.07	-0	0.003	-0.04	-0.16	-0.14	CM	-0.8	-0.95
26	ΔCL	0.148	0.168	0.032	-0.025	0.028	0.302	0.262	CL	1.344	1.646
	ΔCD	0.106	0.1	0.094	0.042	0.126	0.198	0.192	CD	1.386	1.584
	ΔCM	-0.14	-0.16	-0.05	0	-0.08	-0.3	-0.25	CM	-0.85	-1.15